




Cite this: *Dalton Trans.*, 2025, **54**, 908

Received 26th November 2024,
Accepted 11th December 2024

DOI: 10.1039/d4dt03305a

rsc.li/dalton

Deconvoluting capping ligand influence on photophysical properties in tetrathiafulvalene-based diradicaloids†

Nathan E. Lopez,‡ Lauren E. McNamara,  ‡ Sophie W. Anferov and John S. Anderson  *

Tetrathiafulvalene-2,3,6,7-tetrathiolate (TTFtt) complexes are synthetically tunable and emit brightly in the near-infrared II region (NIR II, 1000–1700 nm). Their emission/absorption energies respond to the identity of the capping ligands on the metal center, but a detailed understanding of how ligand bonding interactions dictate photophysical properties is key to predictive design optimization. Here we assess the relative influence of ligand π back-bonding versus sigma (σ) donation in these complexes across a new series of olefin- and phosphite-capped complexes. Increasing the backbonding character of peripheral ligands results in a hypsochromic shift in the absorption maxima, while stronger σ donation results in a bathochromic shift.

Introduction

The high depth penetration in tissue and improved spatial and temporal resolution of NIR II emitters make them promising for use in a wide variety of medical applications, including image-assisted surgeries and *in vitro* monitoring of disease progression.^{1–8} Developing dyes with tunable emission may further enable multicolor imaging and enhanced contrast.^{9–12} Beyond biomedical applications, NIR II dyes have attracted attention for use in OLEDs and information storage, with modular photophysical properties also proving advantageous in these areas.^{13–16} Despite these attributes, current leading NIR II dyes require elaborate scaffolds which are difficult to systematically modify.^{1–3,17–22} Our laboratory has recently reported a compact, modular TTFtt scaffold that absorbs and emits in the NIR II region.^{23,24} These molecules are also diradicals which further broadens their potential applications in fields such as quantum information science.^{25–29} Systematic

changes to the electron-donating or -withdrawing character of capping triarylphosphine ligands results in predictive changes in photophysical properties; absorption and emission shift hypsochromically with increasing Hammett parameter.^{23,24} Diradical character is also responsive to the capping metal/ligand combination.²⁵ While these examples demonstrate the tunability of this system, the explored span of capping ligand types is comparatively small and there is no clarity on the key interactions that determine shifts in absorption/emission. Such a detailed understanding is critical for optimal tuning of this emissive diradicaloid scaffold.

Herein, a new series of Pt-capped TTFtt complexes has been synthesized and characterized to elucidate the relative influence of ligand σ -donation and π -accepting character on photophysical properties. Three new olefin- and three new triarylphosphite-capped PtTTFtt complexes were synthesized to probe a wider array of ligand properties (Fig. 1A). Natural bonding orbital (NBO) calculations provide insight into the relative π acidity (π_b) and σ -donation of these ligands, which is then correlated with observed photophysical properties.³⁰

Results and discussion

Synthesis and characterization of PtTTFtt compounds 1–6

Six new Pt-capped TTFtt analogs were synthesized according to previously established procedures (Fig. 1A, 1–6).^{23,31} Crystallographic characterization reveals no π stacking in the solid state; the dicationic fragments are encapsulated by $\text{BAR}_4^{\text{F}-}$ anions. The central C–C distances in the TTF core of these molecules have previously been shown to correlate with diradical character.²⁵ This distance ranges from 1.38 to 1.44 Å across this series (4 is omitted due to poor bond resolution), suggesting moderate diradical character.^{24,25} Evans method analysis shows magnetic moments ranging from 0.79–2.05 μ_B , further supporting population of a low-lying triplet state (Fig. S14–S19†). We note that while no π stacking is observed in the solid state, TTF fragments are also known to π stack in solution. This may

Department of Chemistry, University of Chicago, Chicago, Illinois, 60637, USA.

E-mail: jsanderson@uchicago.edu

† Electronic supplementary information (ESI) available. CCDC 2377387–2377392.

For ESI and crystallographic data in CIF or other electronic format see DOI: <https://doi.org/10.1039/d4dt03305a>

‡ These authors contributed equally to this work.



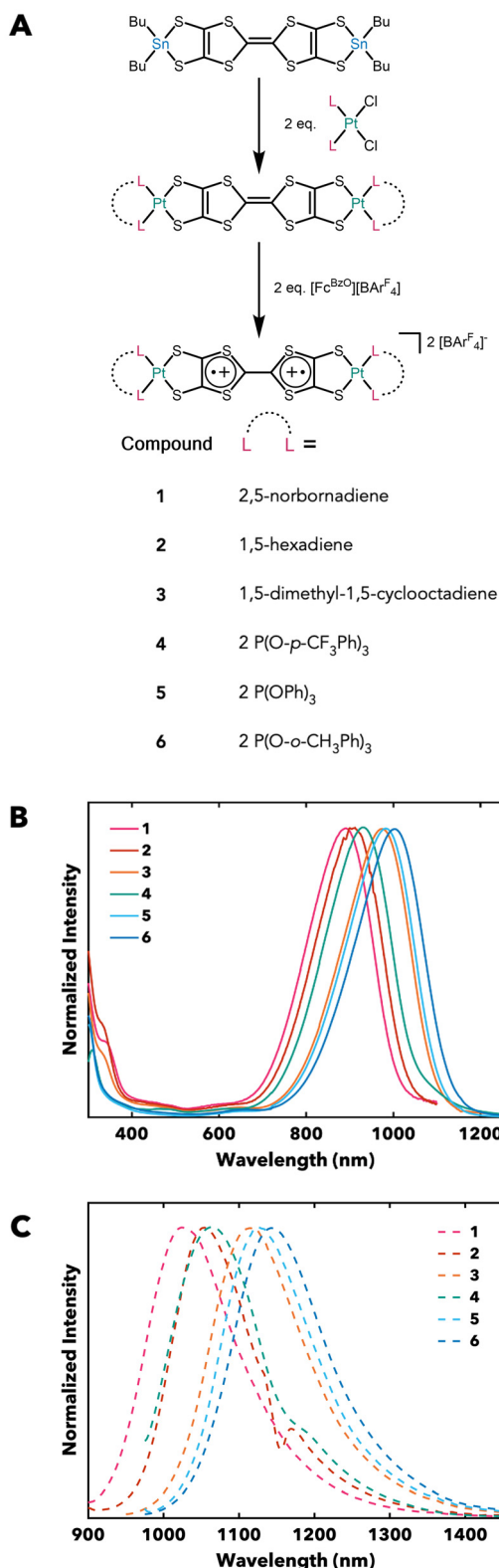


Fig. 1 (A) Synthesis of new Pt-capped TTFt analogs. See ESI† for further details and procedures. BArF_4^- = tetrakis[3,5-bis(trifluoromethyl)phenyl]borate. (B) Absorption of new analogs in dichloromethane (DCM) at 298 K. (C) Photoluminescence (PL) of new analogs in CH_2Cl_2 (2, 4) and CD_2Cl_2 (1, 3, 5, 6) at 298 K.

explain the generally lower magnetic moments in solution than the value expected for a triplet ($2.83\mu_B$). Room temperature CW EPR spectra display a single isotropic feature attributed to an organic radical at $g \approx 2$ that also supports a thermally populated triplet state (Fig. S33–38†).

The UV-vis-NIR spectra of these new compounds in DCM show hypsochromically-shifted absorption maxima compared to previously reported analogs (890–1005 nm, Fig. 1B).^{23,24,31} Compounds 1–6 also emit brightly in DCM, with maxima ranging from 1030–1143 nm (Fig. 1C). The photoluminescence (PL) spectra of compounds 1, 3, 5, and 6 are convoluted by the IR absorption of DCM (which onsets at ~ 1150 nm), so for subsequent analysis, the maxima obtained from the PL spectra of these compounds in CD_2Cl_2 are used. We note what appears to be an anomalously bathochromic shift in the absorption and emission spectra of 3, particularly when compared with the other olefin complexes in this series. However, and as shown below, this is rationalized by the substantially better donor properties of 1,5-dimethyl-1,5-cyclooctadiene.

Photoluminescent quantum yields (PLQYs, ϕ_{PL}) range from 0.36–2.39% (Fig. 2).²⁴ This trend generally follows the predictions of the energy gap law with larger PLQYs exhibited by higher energy-emitting examples. This series also displays high molar extinction coefficients (ϵ) from $\sim 40\,000$ to $90\,000\text{ M}^{-1}\text{ cm}^{-1}$ and correspondingly high brightness values ($\epsilon\phi_{\text{PL}}$) from $\sim 20\,000$ to $70\,000\text{ M}^{-1}\text{ cm}^{-1}$; these brightness values are substantially higher than commercially available NIR II dyes like IR-26.³⁴ Overall, we note that the ϕ_{PL} in these complexes are among the brightest reported values for NIR II-emitting complexes.^{32,33}

Natural bonding orbital (NBO) analysis

After photophysically characterizing complexes 1–6, we then turned to deconvoluting what ligand parameters most accurately predicted these observed photophysical trends. We initially performed a second-order perturbative energy analysis on the precursor LPtCl_2 or L_2PtCl_2 fragments to investigate the strength of π -backbonding and σ -donation equitably (Table 1,

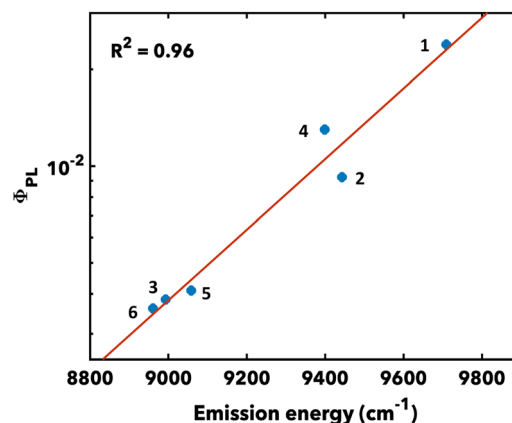


Fig. 2 PLQYs and energy gap law behavior of olefin and phosphite TTFt analogs in DCM at 298 K.



Table 1 Calculated donation-acceptor interaction strengths for the corresponding LPtCl_2 or L_2PtCl_2 fragments and experimental photophysical parameters for the TTFt complexes

	1	2	3	4	5	6	dppe ²³	$\text{P}(p\text{-OMePh})_3$ ²⁴	PPh_3 ³⁵	$\text{P}(p\text{-BrPh})_3$ ²⁴
π_b (kcal mol ⁻¹)	109	100	96	37	40	37	33	27	28	28
σ (kcal mol ⁻¹)	580	559	551	587	556	617	—	—	—	—
λ_{Abs} (nm)	890	914	975	931	984	1005	1044	1130	1100	1059
E_{Abs} (eV)	1.394	1.357	1.272	1.332	1.261	1.234	1.188	1.098	1.128	1.171
λ_{Em} (nm)	1030 ^a	1059	1115 ^a	1064	1127 ^a	1143 ^a	1202	1280	1266	1198
E_{Em} (eV)	1.204	1.171	1.113	1.165	1.101	1.085	1.032	0.969	0.980	1.036
ε (M ⁻¹ cm ⁻¹)	29 520	68 080	87 600	43 350	52 366	63 716	80 000	94 808	107 000	80 868
ϕ_{PL} (%)	2.39	0.92	0.38	1.30	0.41	0.36	0.136	0.041	0.07	0.171
$\varepsilon\phi_{\text{PL}}$ (M ⁻¹ cm ⁻¹)	70 553	62 634	33 288	56 355	21 470	22 937	10 880	3887	7490	13 828

dppe = $[(\text{dppe})\text{Pt}]_2\text{TTFt}[\text{BAR}_4^{\text{F}}]_2$, $\text{P}(p\text{-OMePh})_3 = [(\text{P}(p\text{-OMePh})_3)\text{Pt}]_2\text{TTFt}[\text{BAR}_4^{\text{F}}]_2$, $\text{PPh}_3 = [(\text{PPh}_3)_2\text{Pt}]_2\text{TTFt}[\text{BAR}_4^{\text{F}}]_2$, $\text{P}(p\text{-BrPh})_3 = [(\text{P}(p\text{-BrPh})_3)_2\text{Pt}]_2\text{TTFt}[\text{BAR}_4^{\text{F}}]_2$ in CH_2Cl_2 . ^a Value taken from fluorescence spectrum taken in CD_2Cl_2

Table S7,† and Fig. 3).³⁰ The strengths of π -backbonding interactions are ~ 28 kcal mol⁻¹ for triarylphosphines, ~ 40 kcal mol⁻¹ for triarylphosphites, and ~ 100 kcal mol⁻¹ for olefins respectively. As expected, this analysis reveals that phosphites are stronger π -acids than previously examined phosphine ligands. More interestingly, phosphites are worse π -acids but

comparable σ -donors to olefins. The strength of σ -donation from olefin C–C π bonds or P lone pairs to Pt–Cl antibonding orbitals spans a similar range of 540–620 kcal mol⁻¹ for olefins and phosphites. The strength of these interactions is rationalized through the orbital overlap between donor orbitals (Pt 5d, P lone pair, or olefin C–C π) and accepting orbitals (Pt–Cl σ^* , P–O σ^* , or C–C π^*). Examples of these interactions are depicted in Fig. 3. While the σ interaction appears to have comparable overlap between the olefins and phosphites, the C–C π^* orbitals point more directly at the Pt 5d orbitals than the phosphite's P–O σ^* , yielding a much stronger computed backbonding energy. Most importantly, the ability to quantify the relative ligand interactions across this series of complexes on one energetic scale enables us to analyze what ligand features correlate most closely with the observed photophysical properties.

Regressions of the absorption and emission energy against ligand parameters were performed to understand what factors held the greatest predictive value. Both the phosphite and olefin complexes form their own independent sets when only π -backbonding interactions are considered, suggesting that some σ -effects must be considered (Fig. S48†). A weighted average of backbonding and σ -donation was used to address this possibility: $A_{\text{fit}} = a\pi_b + (1 - a)\sigma + c$ (a is a weight ranging from 0 to 1 and A is the predicted absorption or emission energy). This analysis results in a satisfactory trend with absorption when the weighted average was comprised of 4 : 1 π -backbonding : σ -donation (79 and 21% respectively) with $R^2 = 0.93$ (Fig. 4A). Similarly, an analysis for the emission maxima of these compounds results in a clear trend with an identical weight ($a = 0.79$ and $R^2 = 0.94$, Fig. 4B). Finally, we note some anomalies in these analyses. Namely, while complex 4 possesses similar donation strength to the other phosphites, its absorption and emission are much more hypsochromically shifted. From a statistical analysis, the absorption/emission of 4 is >1 standard deviation from the mean, so it was removed from the dataset in all analyses. We suspect this anomalous behavior for 4 arises from solution-phase fluorophilic interactions with the BAR_4^{F} anions as similar outlier behavior has been observed in CF_3 and F derivatives of other Pt-capped TTFt complexes.²⁴

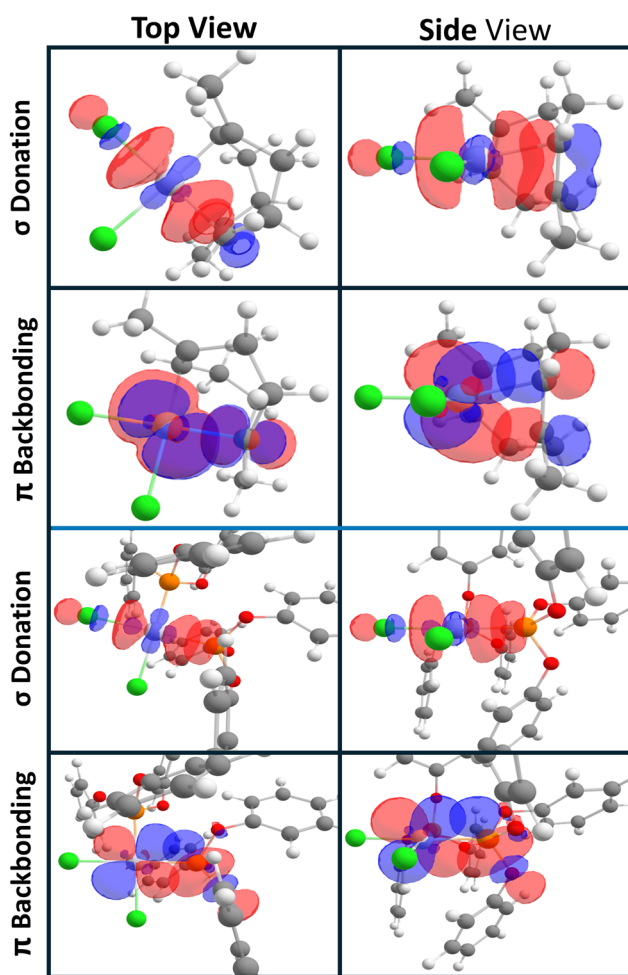


Fig. 3 Top and side view visualization of σ and π_b interaction of the chloride analogs of **3** (above blue line) and **5** (below blue line).



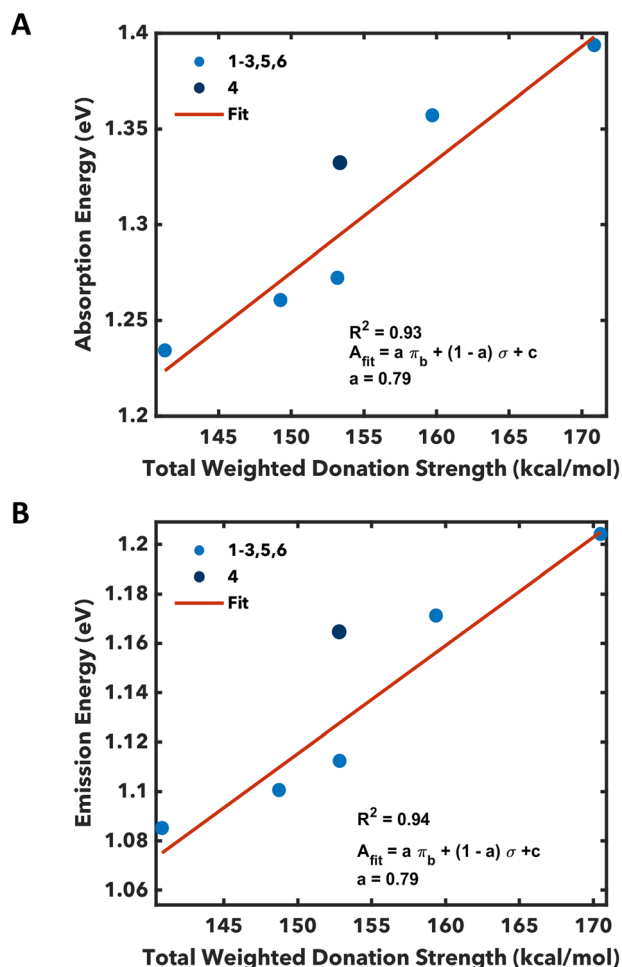


Fig. 4 Trendline of weighted donation strengths for the L_2PtCl_2 or LPtCl_2 fragments and (A) energy of absorption maximum and (B) energy of emission maxima for 1, 2, and 4 in DCM and 3, 5, and 6 in CD_2Cl_2 .

While backbonding alone is insufficient in predicting photophysical properties of Pt-capped TTFtt complexes it still constitutes the majority of the predictive power in this model. We extended this analysis to include some previously reported phosphines (Table 1, Fig. S48 and 49†). We qualitatively observe that the bathochromically shifted features in phosphine-capped PtTTFtt compounds can be attributed to comparatively low backbonding character. Our observations here support previous time-dependent density functional theory (TD-DFT) analyses with phosphine-capped PtTTFtt complexes where increased donation strength of the phosphines results in a better energetic overlap between the Pt-ligand fragment and TTF core. This better overlap results in increased delocalization and bathochromically-shifted absorption and emission maxima.²⁴ Similarly, an increase in π -backbonding from Pt to the capping ligands destabilizes this fragment relative to the TTF core, resulting in a poorer energetic overlap, less delocalization, and a hypsochromic shift. Meanwhile, σ -donation has a smaller but still significant effect.

Conclusions

Six new Pt-capped TTFtt compounds that absorb and emit in the NIR II region have been synthesized and characterized. The π -backbonding and σ -donation of the capping ligands in these complexes have been computed with second-order perturbative analysis within an NBO method. Trends between π -backbonding and σ -donation inform that the absorption and emission maxima is dominated by the strength of the backbonding interaction between Pt and its capping ligand. However, comparing these new complexes with previously reported phosphine analogs shows that backbonding alone is an insufficient predictor, and consideration of σ -donation is required. We find that the optimal weighting is $\sim 80\% : 20\%$ π_b/σ for the phosphite and olefin analogs. These results quantify an intuitive and synthetically facile method of tuning the photophysical properties of Pt-capped TTFtt complexes through modulation of the π -accepting character of the capping ligands.

Experimental

General considerations

All syntheses were performed under dry N_2 in an MBraun UNILab glovebox. Midwest Microlabs conducted all elemental analyses (C, H, N). All solvents were dried and N_2 -purged on a Pure Process Technology solvent system, filtered through activated alumina, and stored over 4 Å molecular sieves. TTFtt (SnBu_2)₂,³¹ $[\text{Fc}^{\text{BzO}}][\text{BAR}^{\text{F}}_4]$,³¹ $\text{P}(\text{O}-o\text{-CH}_3\text{Ph})_3$,³⁶ $\text{Pt}\{\text{P}(\text{O}-p\text{-CF}_3\text{Ph})_3\}_2\text{Cl}_2$,³⁷ $\text{Pt}\{\text{P}(\text{O}-o\text{-CH}_3\text{Ph})_3\}_2\text{Cl}_2$,³⁷ $\text{Pt}(\text{NBD})\text{Cl}_2$,³⁸ $\text{Pt}(\text{HEX})\text{Cl}_2$,³⁸ and $\text{Pt}(\text{Me}_2\text{COD})\text{Cl}_2$ ³⁸ were prepared according to literature procedures (NBD = 2,5-norbornadiene, HEX = 1,5-hexadiene, and Me_2COD = 1,5-dimethyl-1,5-cyclooctadiene). All other chemicals and reagents were purchased from commercial sources and used as received.

Synthesis

$[\{\text{NBDPt}\}_2\text{TTFtt}][\text{BAR}^{\text{F}}_4]_2$ (1). TTFtt(SnBu_2)₂ (0.016 g, 0.02 mmol) was dissolved in 2 mL DCM and added dropwise to a solution of $\text{Pt}(\text{NBD})\text{Cl}_2$ (0.015 g 0.04 mmol) in 2 mL of DCM. The mixture turned deep red-orange, and the suspension was allowed to stir for 10 min. Then, $[\text{Fc}^{\text{BzO}}][\text{BAR}^{\text{F}}_4]$ (0.050 mg 0.04 mmol) in 3 mL DCM was added slowly to the reaction mixture. The reaction slowly turned from dark red-orange to green-brown and after stirring for 5 min, the solution was concentrated to 1 mL under vacuum. While stirring, 5 mL petroleum ether was added slowly, and dichroic green-brown crystals formed. The crystals were washed with petroleum ether (3 × 5 mL) and dried under vacuum. The crude product was redissolved in 1 mL of DCM, filtered through Celite, and layered with petroleum ether. The layered solution was placed in a -35°C freezer and allowed to recrystallize overnight, yielding dichroic green-brown crystals (0.040 g, 70%) suitable for SXRD. ^1H NMR (400 MHz, CD_2Cl_2 , 298 K) δ 1.92 (bm, NBD 7-H), 4.40 (bm, NBD 1-H, 4-H), 5.63 (bm, NBD



=CH), 7.55 (bs, [BAR^F₄][−]), 7.72 (bs, [BAR^F₄][−]). We note due to the air-sensitive nature of this compound, we did not run elemental analysis. See NMR and crystal structure for purity and composition/connectivity, respectively.

[(HEXPt)₂TTFtt][BAR^F₄]₂ (2). TTFtt(SnBu₂)₂ (0.065 g, 0.08 mmol) was dissolved in 3 mL DCM and added dropwise to a solution of Pt(HEX)Cl₂ (0.057 g, 0.16 mmol) in 3 mL of DCM. The mixture turned deep red-brown, and the suspension was allowed to stir for 10 min. Then, [Fc^{BzO}][BAR^F₄] (0.200 g, 0.17 mmol) in 4 mL DCM was added slowly to the reaction mixture. The reaction slowly turned from dark red-brown to green-brown and after stirring for 5 min, the solution was concentrated to 1 mL under vacuum. While stirring, 5 mL petroleum ether was added slowly, and dichroic blue-brown crystals formed. The crystals were washed with petroleum ether (3 × 5 mL) and dried under vacuum. The crude product was redissolved in 2 mL of DCM, filtered through Celite, and layered with petroleum ether. The layered solution was placed in a −35 °C freezer and allowed to recrystallize overnight, yielding dichroic blue-brown crystals (0.146 g, 69%) suitable for SXRD. ¹H NMR (400 MHz, CD₂Cl₂, 298 K) δ 2.80 (bm, HEX CH₂), 4.26–4.30 (bd, HEX =CH₂ (Z)), 5.07 (bd, HEX =CH₂ (E)), 5.93 (bm, HEX =CH), 7.57 (s, [BAR^F₄][−]), 7.73 (s, [BAR^F₄][−]). Anal. calcd for 2, C₈₂H₄₄B₂F₄₈Pt₂S₈: C 37.74%, H 1.70%, N 0%; found: C 37.73%, H 1.87%, N none.

[(Me₂CODPt)₂TTFtt][BAR^F₄]₂ (3). TTFtt(SnBu₂)₂ (0.050 g, 0.06 mmol) was dissolved in 3 mL DCM and added dropwise to a solution of Pt(Me₂COD)Cl₂ (0.051 g 0.13 mmol) in 3 mL of DCM. The solution turned dark brown, and was allowed to stir for 10 min. Then, [Fc^{BzO}][BAR^F₄] (0.175 g 0.15 mmol) in 4 mL DCM was added slowly to the dark brown solution. The reaction slowly turned from dark brown to green and after stirring for 5 min, the solution was concentrated to 1 mL under vacuum. While stirring, 5 mL petroleum ether was added slowly, and green crystals formed. The crystals were washed with petroleum ether (3 × 5 mL) and dried under vacuum. The crude product was redissolved in 2 mL of DCM, filtered through Celite, and layered with hexanes. The layered solution was placed in a −35 °C freezer and allowed to recrystallize for two months, yielding green crystals (0.088 g, 52%) suitable for SXRD. ¹H NMR (400 MHz, CD₂Cl₂, 298 K) δ 2.14 (bs, Me₂COD CH₃), 2.48 (bm, Me₂COD CH₂), 2.55 (bm, Me₂COD CH₂), 2.71 (bm, Me₂COD CH₂), 5.54 (bm, Me₂COD =CH), 7.56 (s, [BAR^F₄][−]), 7.72 (s, [BAR^F₄][−]). Anal. calcd for 3, C₉₀H₅₆B₂F₄₈Pt₂S₈: C 39.77%, H 2.08%, N 0%; found: C 40.10%, H 2.07%, N none.

[(P(O-*p*-CF₃Ph)₃)₂Pt]₂TTFtt][BAR^F₄]₂ (4). TTFtt(SnBu₂)₂ (0.050 g, 0.06 mmol) was dissolved in 4 mL CH₂Cl₂ and added dropwise to a solution of Pt{P(O-*p*-CF₃Ph)₃}Cl₂ (0.155 g, 0.12 mmol) in 3 mL of CH₂Cl₂. The solution turned deep red and the suspension was allowed to stir for 10 min. Then, [Fc^{BzO}][BAR^F₄] (0.165 g, 0.132 mmol) in 4 mL CH₂Cl₂ was added slowly to the reaction mixture. The solution slowly turned from red to green and after stirring for 5 min, the solution was concentrated to 1 mL under vacuum. While stirring, 5 mL petroleum ether was added slowly, and green crystals formed. The crystals were washed with petroleum ether (3 ×

3 mL) and dried under vacuum. The crude product was redissolved in 1 mL of CH₂Cl₂, filtered through Celite, and layered with petroleum ether. The layered solution was placed in a −35 °C freezer and allowed to recrystallize overnight, yielding green crystals (0.235 g, 87%) suitable for SXRD. ¹H NMR (400 MHz, CD₂Cl₂, 298 K) δ 7.19 (d, Ar-H), 7.53 (s, [BAR^F₄][−]), 7.63 (d, Ar-H), 7.73 (s, [BAR^F₄][−]). ³¹P{¹H} NMR (162 MHz, CD₂Cl₂, 298 K) δ 73.57 (*J*_{Pt-P} = 2400 Hz). Anal. calcd for 4, C₁₅₄H₇₂O₁₂P₄B₂F₆₀Pt₂S₈: C 41.08%, H 1.62%, N 0%; found: C 41.38%, H 1.71%, N none.

[(P(OPh)₃)₂Pt]₂TTFtt][BAR^F₄]₂ (5). TTFtt(SnBu₂)₂ (0.033 g, 0.04 mmol) was dissolved in 4 mL CH₂Cl₂ and added dropwise to a solution of Pt{P(OPh)₃}Cl₂ (0.078 g, 0.08 mmol) in 3 mL of CH₂Cl₂. The solution turned dark red and was allowed to stir for 10 min. Then, [Fc^{BzO}][BAR^F₄] (0.101 g, 0.088 mmol) in 4 mL CH₂Cl₂ was added slowly to the reaction mixture. The solution slowly turned from red to dark green and after stirring for 5 min, the solution was concentrated to 1 mL under vacuum. While stirring, 5 mL petroleum ether was added slowly and green crystals formed. The crystals were washed with petroleum ether (3 × 3 mL) and dried under vacuum. The crude product was redissolved in 1 mL of CH₂Cl₂, filtered through Celite, and layered with petroleum ether. The layered solution was placed in a −35 °C freezer and allowed to recrystallize overnight, yielding green crystals (0.108 g, 73%) suitable for SXRD. ¹H NMR (400 MHz, CD₂Cl₂, 298 K) δ 7.07 (d, Ar-H), 7.29 (m, Ar-H), 7.55 (s, [BAR^F₄][−]), 7.73 (s, [BAR^F₄][−]). ³¹P{¹H} NMR (162 MHz, CD₂Cl₂, 298 K) δ 70.91. Anal. calcd for 5, C₁₄₂H₈₄O₁₂P₄B₂F₄₈Pt₂S₈: C 46.26%, H 2.30%, N 0%; found: C 46.14%, H 2.54%, N none.

[(P(O-*o*-CH₃Ph)₃)₂Pt]₂TTFtt][BAR^F₄]₂ (6). TTFtt(SnBu₂)₂ (0.050 g, 0.06 mmol) was dissolved in 4 mL CH₂Cl₂ and added dropwise to a solution of Pt{P(O-*o*-CH₃Ph)₃}Cl₂ (0.116 g, 0.12 mmol) in 3 mL of CH₂Cl₂. The solution turned deep purple and was allowed to stir for 10 min. Then, [Fc^{BzO}][BAR^F₄] (0.165 g, 0.132 mmol) in 4 mL CH₂Cl₂ was added slowly to the reaction mixture. The solution slowly turned from purple to green and after stirring for 5 min, the solution was concentrated to 1 mL under vacuum. While stirring, 5 mL petroleum ether was added slowly and green crystals formed. The crystals were washed with petroleum ether (3 × 3 mL) and dried under vacuum. The crude product was redissolved in 1 mL of CH₂Cl₂, filtered through Celite, and layered with petroleum ether. The layered solution was placed in a −35 °C freezer and allowed to recrystallize overnight, yielding green crystals (0.171 g, 74%) suitable for SXRD. ¹H NMR (400 MHz, CD₂Cl₂, 298 K) δ 1.98 (s, CH₃), 7.01–7.17 (m, Ar-H), 7.55 (s, [BAR^F₄][−]), 7.73 (s, [BAR^F₄][−]). ³¹P{¹H} NMR (162 MHz, CD₂Cl₂, 298 K) δ 68.86 (*J*_{Pt-P} = 2431 Hz). We note that we were not able to resolve *J*_{Pt-P} coupling for this compound. Anal. calcd for 6, C₁₅₄H₁₀₈O₁₂P₄B₂F₄₈Pt₂S₈: C 47.98%, H 2.83%, N 0%; found: C 48.08%, H 3.03%, N none.

Author contributions

Conceptualization: N. E. L., L. E. M., and J. S. A.; investigation and formal analysis: N. E. L., L. E. M., and S. W. A.; visualiza-



tion: N. E. L., L. E. M., S. W. A. and J. S. A.; supervision: J. S. A.; all authors contributed to the writing of this work.

Data availability

Crystallographic data for 1–6 has been deposited at the CCDC under 2377387, 2377388, 2377289, 2377390, 2377391, 2377392† and can be obtained from <https://www.ccdc.cam.ac.uk/structures/>.

Conflicts of interest

J. S. A. and L. E. M. have a patent filed on this work.

Acknowledgements

This work was supported by the U.S. Department of Energy, Office of Science, Office of Basic Energy Sciences, under Grant DE-SC0019215, and the Army Research Office under Grant W911NF-23-1-0233. This work was done, in part, at the Chicago MRSEC, which is funded by the NSF through Grant DMR-1420709. Parts of this work were performed at the Soft Matter Characterization Facility at the Pritzker School of Molecular Engineering at the University of Chicago. We are grateful for the computational resources were supplied by the UChicago Computing Center. N.J., J.S.S., P.M.C., and C-Y. L. are thanked for helpful discussions.

References

- G. Hong, A. L. Antaris and H. Dai, *Nat. Biomed. Eng.*, 2017, **1**, 1–22.
- A. Matsui, E. Tanaka, H. S. Choi, J. H. Winer, V. Kianzad, S. Gioux, R. G. Laurence and J. V. Frangioni, *Surgery*, 2010, **148**, 87–95.
- B. Li, M. Zhao, L. Feng, C. Dou, S. Ding, G. Zhou, L. Lu, H. Zhang, F. Chen, X. Li, G. Li, S. Zhao, C. Jiang, Y. Wang, D. Zhao, Y. Cheng and F. Zhang, *Nat. Commun.*, 2020, **11**, 3102.
- Y. Chen, Y. Yang and F. Zhang, *Nat. Protoc.*, 2024, 1–22.
- L.-Y. Huang, S. Zhu, R. Cui and M. Zhang, *Anal. Chem.*, 2020, **92**, 535–542.
- Y. Song, G. Yu, B. Xie, K. Zhang and F. Huang, *Appl. Phys. Lett.*, 2020, **117**, 093302.
- J.-J. Wu, X.-D. Wang and L.-S. Liao, *ACS Photonics*, 2019, **6**, 2590–2599.
- C.-L. Ho, H. Li and W.-Y. Wong, *J. Organomet. Chem.*, 2014, **751**, 261–285.
- Y. Yang, Y. Chen, P. Pei, Y. Fan, S. Wang, H. Zhang, D. Zhao, B.-Z. Qian and F. Zhang, *Nat. Nanotechnol.*, 2023, **18**, 1195–1204.
- D. Xu, J. Ge, Y. An, S. Bai, Z. Wang, S. Wu, Q. Dai, Z. Lu and G. Liu, *Small*, 2023, **19**, 2300859.
- J. Xu, N. Zhu, Y. Du, T. Han, X. Zheng, J. Li and S. Zhu, *Nat. Commun.*, 2024, **15**, 2845.
- S. Zhu, S. Herraiz, J. Yue, M. Zhang, H. Wan, Q. Yang, Z. Ma, Y. Wang, J. He, A. L. Antaris, Y. Zhong, S. Diao, Y. Feng, Y. Zhou, K. Yu, G. Hong, Y. Liang, A. J. Hsueh and H. Dai, *Adv. Mater.*, 2018, **30**, 1705799.
- B. Wang, Z. Chen, X. Li, J. Zhou and Q. Zeng, *J. Alloys Compd.*, 2020, **812**, 152119.
- H. Zhang, Y. Fan, P. Pei, C. Sun, L. Lu and F. Zhang, *Angew. Chem., Int. Ed.*, 2019, **58**, 10153–10157.
- J.-L. He, F.-C. Kong, B. Sun, X.-J. Wang, Q.-S. Tian, J. Fan and L.-S. Liao, *Chem. Eng. J.*, 2021, **424**, 130470.
- Y. Xiao, H. Wang, Z. Xie, M. Shen, R. Huang, Y. Miao, G. Liu, T. Yu and W. Huang, *Chem. Sci.*, 2022, **13**, 8906–8923.
- S. He, S. He, J. Song, J. Song, J. Qu, J. Qu, Z. Cheng and Z. Cheng, *Chem. Soc. Rev.*, 2018, **47**, 4258–4278.
- A. L. Antaris, H. Chen, S. Diao, Z. Ma, Z. Zhang, S. Zhu, J. Wang, A. X. Lozano, Q. Fan, L. Chew, M. Zhu, K. Cheng, X. Hong, H. Dai and Z. Cheng, *Nat. Commun.*, 2017, **8**, 15269.
- X. Zeng, Y. Xiao, J. Lin, S. Li, H. Zhou, J. Nong, G. Xu, H. Wang, F. Xu, J. Wu, Z. Deng and X. Hong, *Adv. Healthcare Mater.*, 2018, **7**, 1800589.
- C. Qu, Y. Xiao, H. Zhou, B. Ding, A. Li, J. Lin, X. Zeng, H. Chen, K. Qian, X. Zhang, W. Fang, J. Wu, Z. Deng, Z. Cheng and X. Hong, *Adv. Opt. Mater.*, 2019, **7**, 1900229.
- J. Ding, M. Zhang, Y. Gao, C. Lu, M. Zhang and F. Li, *J. Phys. Chem. Lett.*, 2023, **14**, 8244–8250.
- L. Wang, N. Li, W. Wang, A. Mei, J. Shao, W. Wang and X. Dong, *ACS Nano*, 2024, **18**, 4683–4703.
- L. E. McNamara, J.-N. Boyn, C. Melnychuk, S. W. Anferov, D. A. Mazziotti, R. D. Schaller and J. S. Anderson, *J. Am. Chem. Soc.*, 2022, **144**, 16447–16455.
- L. E. McNamara, J.-N. Boyn, S. W. Anferov, A. S. Filatov, M. W. Maloney, D. A. Mazziotti, R. D. Schaller and J. S. Anderson, *J. Am. Chem. Soc.*, 2024, **146**, 17285–17295.
- J.-N. Boyn, L. E. McNamara, J. S. Anderson and D. A. Mazziotti, *J. Phys. Chem. A*, 2022, **126**, 3329–3337.
- J. H. Cole and L. C. L. Hollenberg, *Nanotechnology*, 2009, **20**, 495401.
- L. T. Hall, J. H. Cole, C. D. Hill and L. C. L. Hollenberg, *Phys. Rev. Lett.*, 2009, **103**, 220802.
- L. T. Hall, C. D. Hill, J. H. Cole and L. C. L. Hollenberg, *Phys. Rev. B: Condens. Matter Mater. Phys.*, 2010, **82**, 045208.
- J. Köhler, *Phys. Rep.*, 1999, **310**, 261–339.
- A. Comas-Vives and J. N. Harvey, *Eur. J. Inorg. Chem.*, 2011, **2011**, 5025–5035.
- J. Xie, J.-N. Boyn, A. S. Filatov, A. J. McNeece, D. A. Mazziotti and J. S. Anderson, *Chem. Sci.*, 2020, **11**, 1066–1078.
- R. Englman and J. Jortner, *Mol. Phys.*, 1970, **18**, 145–164.
- Q. Yang, H. Ma, Y. Liang and H. Dai, *Acc. Mater. Res.*, 2021, **2**, 170–183.
- S. Hatami, C. Würth, M. Kaiser, S. Leubner, S. Gabriel, L. Bahrig, V. Lesnyak, J. Pauli, N. Gaponik, A. Eychmüller and U. Resch-Genger, *Nanoscale*, 2014, **7**, 133–143.



- 35 L. E. McNamara, C. Melnychuk, J.-N. Boyn, S. W. Anferov, D. A. Mazziotti, R. D. Schaller and J. S. Anderson, *Chem*, 2024, **10**, 2266–2282.
- 36 Y. D. Bidal, C. A. Urbina-Blanco, A. Poater, D. B. Cordes, A. M. Z. Slawin, L. Cavallo and C. S. J. Cazin, *Dalton Trans.*, 2019, **48**, 11326–11337.
- 37 A. L. Fuller, F. R. Knight, A. M. Z. Slawin and J. D. Woollins, *Eur. J. Inorg. Chem.*, 2010, **2010**, 4034–4043.
- 38 A. Lüning, M. Neugebauer, V. Lingen, A. Krest, K. Stirnat, G. B. Deacon, P. R. Drago, I. Ott, J. Schur, I. Pantenburg, G. Meyer and A. Klein, *Eur. J. Inorg. Chem.*, 2015, **2015**, 226–239.

